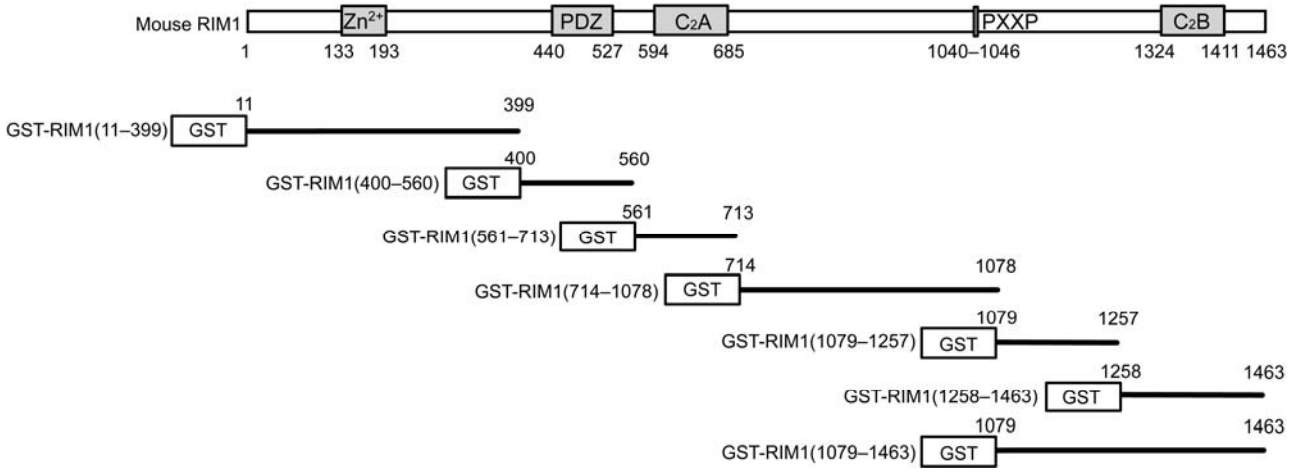

Supplementary Figure 1 Recombinant constructs of GST fusion RIM1 subfragments.

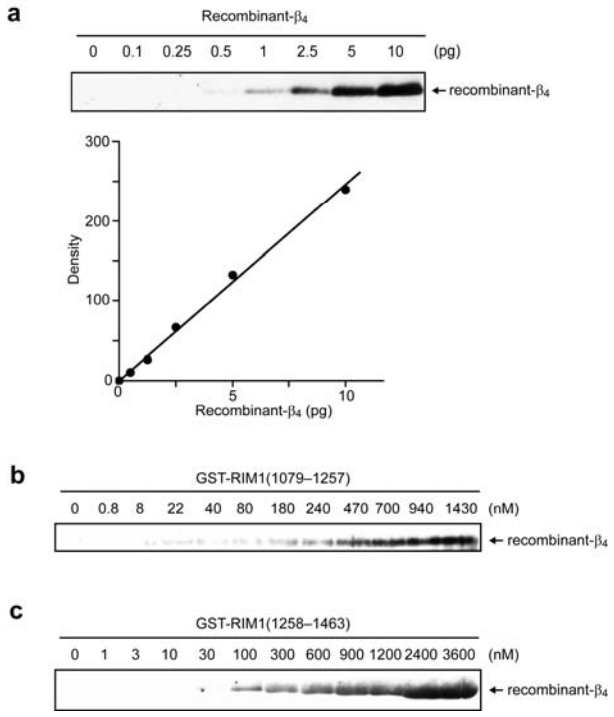

Supplementary Figure 2 *in vitro* binding of the purified RIM1 GST fusion and recombinant β_4 proteins. (**a**) Intensity of recombinant β_4 detected by enhanced chemiluminescence is proportional to the amount of β_4, supporting that this assay is appropriate for quantitative analyses of RIM1-β_4 binding. (**b**) Dose-dependent binding of GST-RIM1(1079-1257) to the recombinant β_4-subunit. (**c**) Dose-dependent binding of GST-RIM1(1258-1463) to the recombinant β_4-subunit.

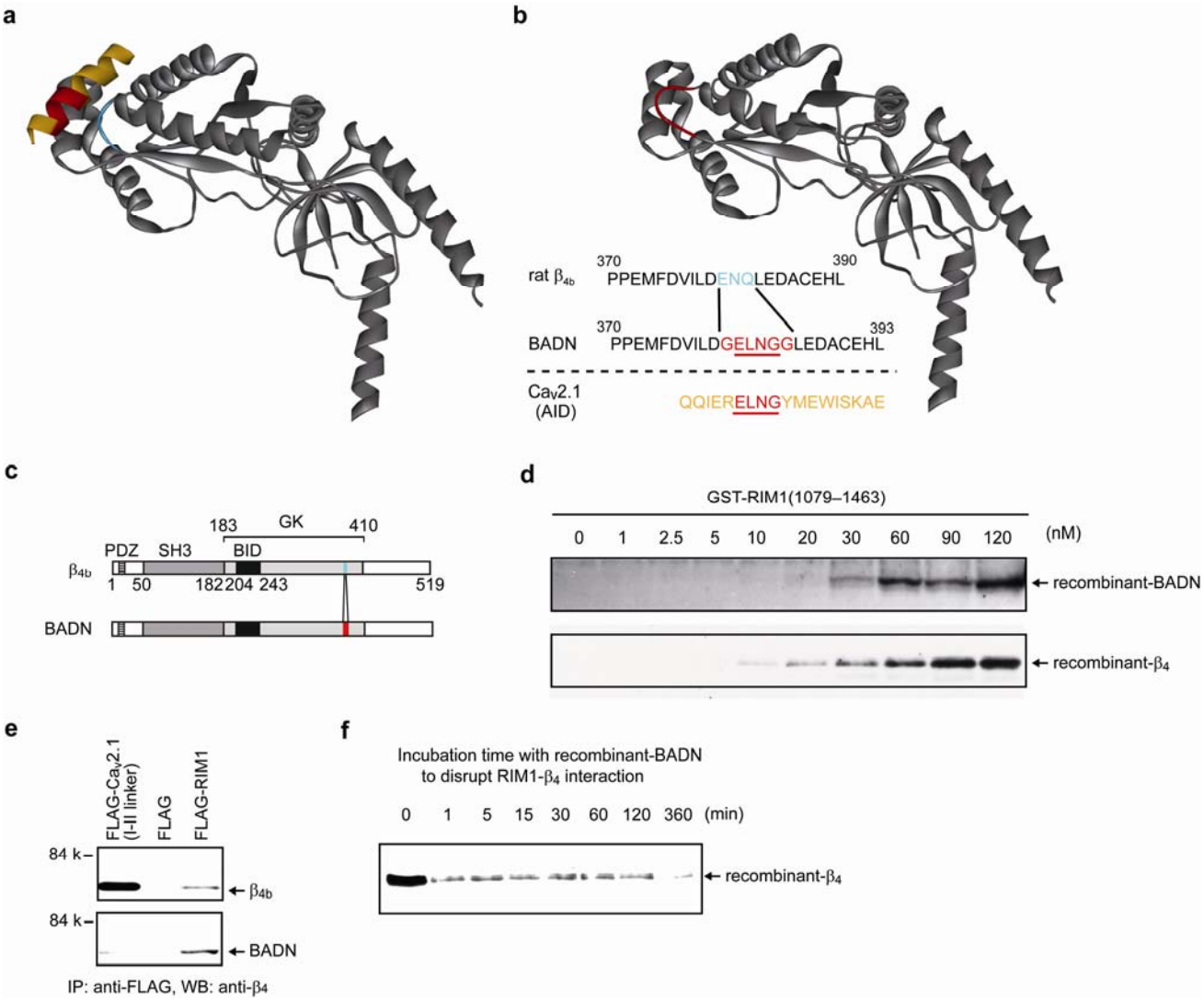

Supplementary Figure 3 Molecular modeling and functional characterization of BADN as a dominant-negative mutant for RIM1 function. (**a**) X-ray structure of the β-subunit and AID (yellow and red) complex adapted from the previous paper by Opatowsky et al[33]. (**b**) Energetically minimized structure of BADN by molecular modeling. BADN is designed to suppress AID binding without destruction of the β-subunit 3D structure. Inset indicates the amino acid sequence (370-393) of BADN compared with the sequence of rat β_{4b} and the AID sequence of $Ca_v2.1$. BADN is constructed on the basis of rat β_{4b}, and hexa-peptide (GELNGG (red)) containing the essential region (ELNG) for β-subunit binding of AID with flanking glycine residues as spacers replacing the original tri-peptide (ENQ (blue)) to suppress AID binding. (**c**) Domain structure of β_{4b} and BADN. (**d**) Dose-dependent binding of recombinant-BADN to the GST-RIM1(1079-1463) is shown. This result shows that BADN has affinity to RIM1(1079-1463) comparable with that of β_4. (**e**) Interaction of recombinant BADN and RIM1 in HEK293 cells. The interaction is evaluated by IP with anti-FLAG antibody, followed by WB with anti-β_4 antibody. Top: HEK293 cells co-transfected with β_{4b} and FLAG-RIM1. FLAG-$Ca_v2.1$(I-II linker) is used as a positive control. Bottom: HEK293 cells co-transfected with BADN and FLAG-RIM1. (**f**) Rapid disruption of the RIM1-β_{4b} interaction by BADN. The dissociation is measured in the presence of excessive BADN protein (200 nM). This result suggests that virtually complete disruption of the RIM1-β_{4b} interaction is attained within 6 h of incubation.

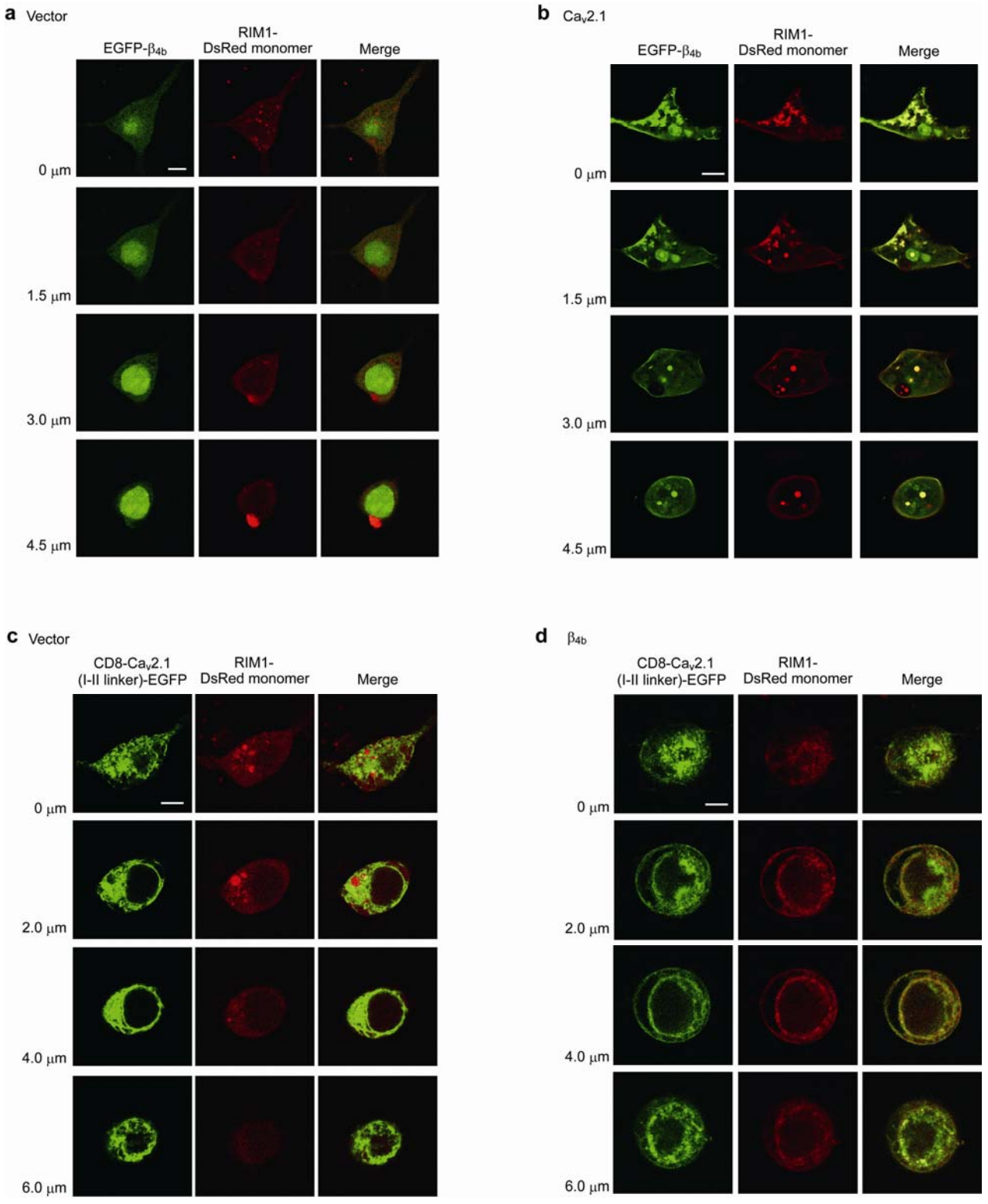

Supplementary Figure 4 Confocal images of RIM1 and β_{4b} colocalization mediated by $Ca_v2.1$ α_1-subunit proteins at the plasma membrane. (**a**) X-Y images at different Z-axis depths in HEK293 cells co-transfected with EGFP-β_{4b} and RIM1-DsRedmonomer in the absence of $Ca_v2.1$. Scale bar: 5 μm. (**b**) X-Y images at different Z-axis depth in of HEK293 cells co-transfected with EGFP-β_{4b} and RIM1-DsRedmonomer in the presence of $Ca_v2.1$. (**c**) X-Y images at different Z-axis depths in HEK293 cells co-transfected with CD8-$Ca_v2.1$(I-II linker)-EGFP and RIM1-DsRedmonomer in the absence of β_{4b}. (**d**) X-Y images at different Z-axis depths in HEK293 cells co-transfected with CD8-$Ca_v2.1$(I-II linker)-EGFP and RIM1-DsRedmonomer in the presence of β_{4b}.

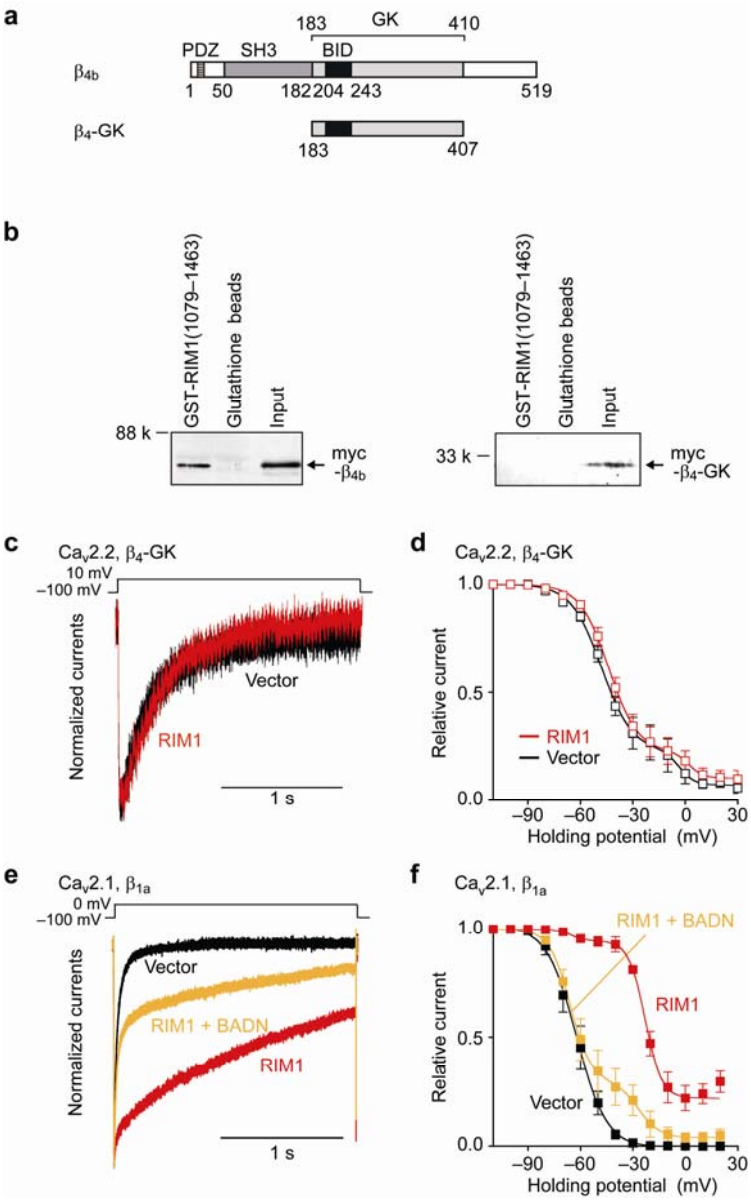

Supplementary Figure 5 Disruption of the RIM1 effects on VDCC inactivation by the β_4 GK domain and BADN. (**a**) Structure of β_4-GK in comparison with the WT β_{4b}. β_4-GK corresponds to 183-407 of rat β_{4b}. (**b**) Pulldown assay of β_4-GK constructs with RIM1(1079-1463) GST fusion protein demonstrates that β_4-GK does not interact with RIM1(1079-1463). cDNA of β_4-GK is subcloned in the expression plasmid pCMV-tag3. GST fusion proteins immobilized on glutathione-Sepharose beads are incubated with cell lysate obtained from myc-β_4-GK-expressing HEK293 cells. Bound proteins are analyzed by WB using anti-myc antibody. (**c**) Inactivation of $Ca_v2.2$ currents in BHK cells expressing $\alpha_2\delta$ and β_4-GK. For comparison of inactivation time courses before and after expression of RIM1 constructs, the peak amplitudes are normalized for Ba^{2+} currents elicited by 2-s pulses to 10 mV from a V_h of –100 mV. 10 mM Ba^{2+} is used as a charge carrier. (**d**) Inactivation curves of $Ca_v2.2$ currents in BHK cells expressing $\alpha_2\delta$ and β_4-GK. (**e**) Dominant-negative effect of BADN for RIM1 effects on inactivation properties of VDCCs. Inactivation kinetics of $Ca_v2.1$ currents in BHK cells expressing $\alpha_2\delta$ and β_{1a}. (**f**) Inactivation curves of $Ca_v2.1$ in BHK cells expressing $\alpha_2\delta$ and β_{1a}. The differences at > –80 mV between vector and RIM1, or those between RIM1 plus BADN and RIM1 are significant ($P < 0.05$).

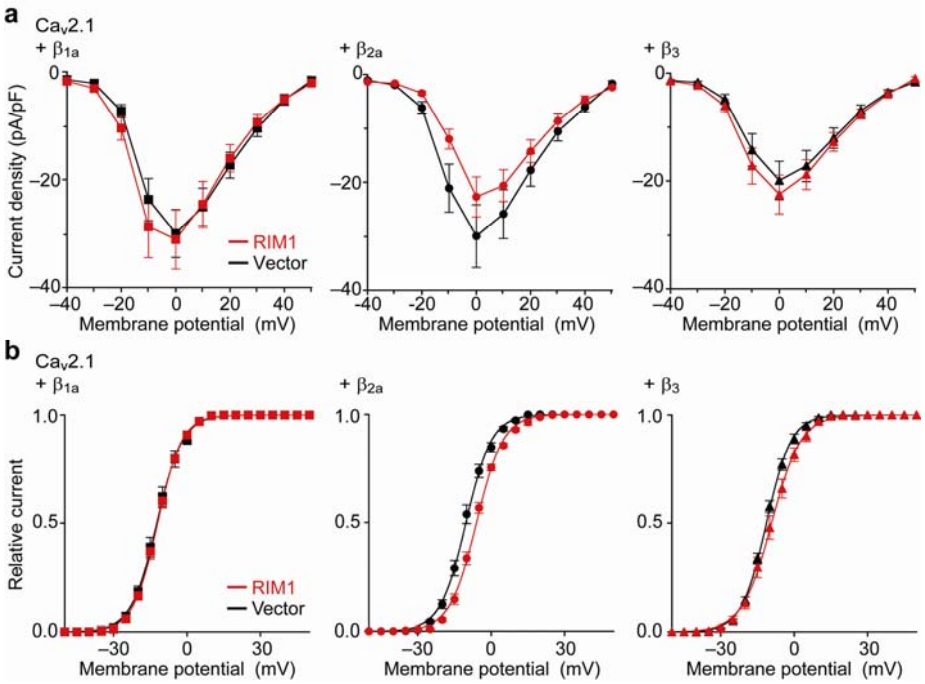

Supplementary Figure 6 Effects of RIM1 on the activation properties of VDCCs. (**a**) *I-V* relationships of $Ca_v2.1$ channels in BHK cells expressing $\alpha_2\delta$ and various β-subunits. The V_h is –100 mV. (**b**) Activation curves. The differences between vector control and RIM1 are significant at membrane potentials from –25 to +5 mV for β_{2a} are significant ($P < 0.05$).

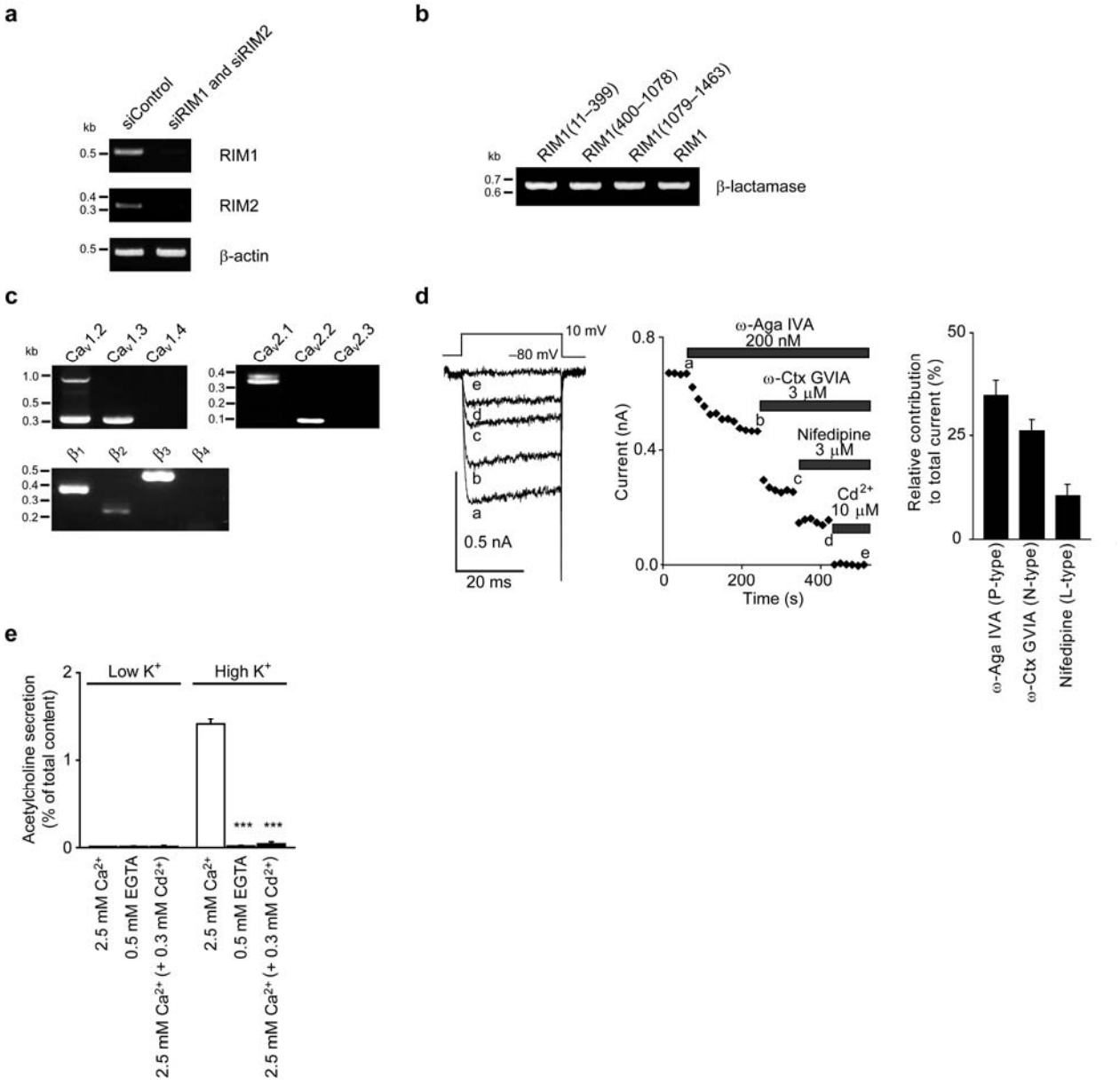

Supplementary Figure 7 Molecular and physiological characterization of PC12 cells. (**a**) RT-PCR analysis of RIM1 and RIM2 RNA expression in PC12 cells treated with GAPDH siRNA (siControl) and combination of RIM1- and RIM2-specific siRNAs (siRIM1 & siRIM2). Primer sequences are indicated in **Supplementary Table 9**. RT-PCR was performed using LA-PCR kit (TaKaRa), according to the manufacturer's information. (**b**) Transfection levels of cDNAs of RIM constructs are examined using PCR in PC12 cells. Primers are designed to amplify the lactamase gene in the pCI-neo vector (**Supplementary Table 9**). PCR was carried out using LA-PCR kit. (**c**) RNA expression analysis of α_1 and β-subunits using RT-PCR in PC12 cells. (**d**) Pharmacological dissection of high voltage-activated Ca^{2+} channel currents in PC12 cells. Left & Middle: time course of blockage of Ca^{2+} current by serial application of 200 nM ω-Aga IVA, 3 μM ω-Ctx GVIA, 3 μM Nifedipine, and 10 μM Cd^{2+} in PC12 cell. Right: summary of relative contributions of each current type. (**e**) Cd^{2+}-sensitive Ca^{2+} influx pathway is responsible for depolarization-dependent ACh release from ChAT-transfected PC12 cells. Cd^{2+} is a selective blocker for high voltage-activated Ca^{2+} channels. $^{***}P < 0.001$ vs 2.5 mM Ca^{2+}.

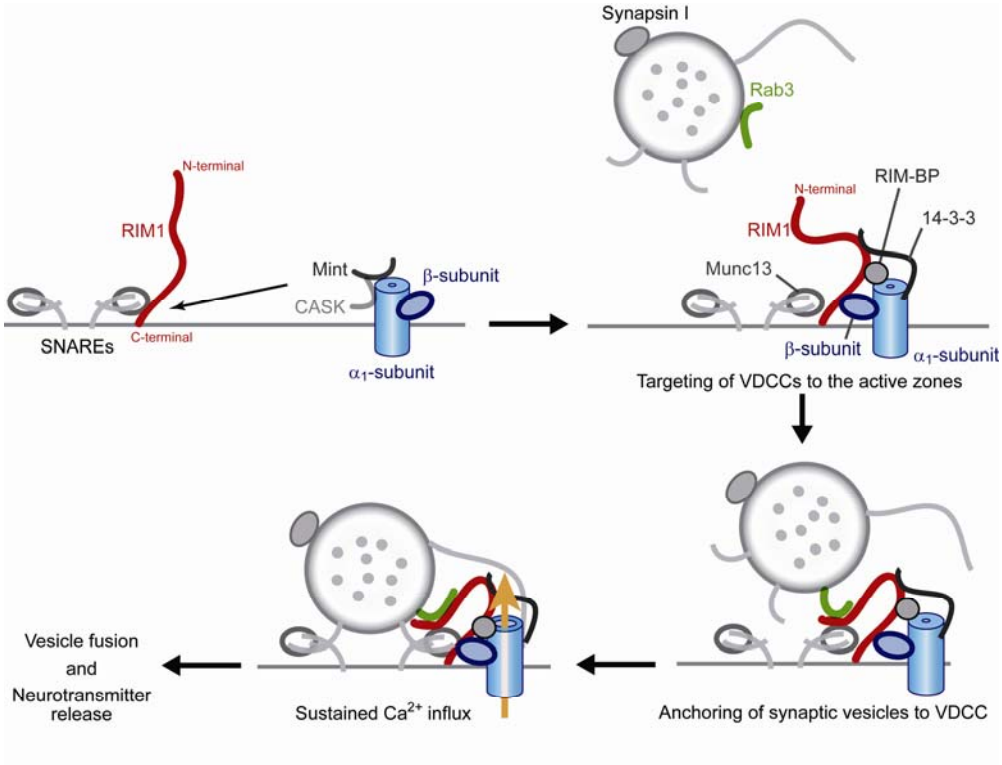

Supplementary Figure 8 A model detailing the putative role of the β-subunit-RIM1 interaction at presynaptic AZs. Synaptic vesicles are anchored to presynaptic AZs through the association of RIM1 with b-subunits, Rab3, and Munc13. Also, functional properties of neuronal VDCCs are significantly modulated by RIM1 through physical association with the b-subunit, which can efficiently maintain Ca^{2+} influx through VDCC at AZs. These presynaptic processes regulated by the RIM1-β complex can involve other important presynaptic proteins such as RIM-BP in the vesicle anchoring by mediating an indirect association of RIM1 with VDCC α_1. 14-3-3, which regulates VDCC inactivation, may contribute to anchoring via the same mechanism. Mint and CASK regulate presynaptic targeting of VDCCs via their association with α_1.

Supplementary Table 1 Effects of RIM1 constructs on current density, activation, and inactivation of $Ca_v2.1$, $Ca_v2.2$, $Ca_v2.3$, or $Ca_v1.2$ channel in BHK cells expressing α_2/δ and β_{4b}[1)].

Subunit combination		Current density (pA / pF)[2)]	Activation parameters			Inactivation parameters					
			$V_{0.5}$ (mV)	k (mV)	τ_{act} (ms)[3)]	a	$V_{0.5}^{1st}$ (mV)	k^{1st} (mV)	b	$V_{0.5}^{2nd}$ (mV)	k^{2nd} (mV)
$Ca_v2.1$	Vector	−14.0 ± 2.9 (15)	−7.2 ± 1.2 (9)	5.7 ± 0.1 (9)	0.53 ± 0.05 (9)	1.00 ± 0.00 (12)	−45.9 ± 1.8 (12)	−7.5 ± 0.3 (12)			
+ β_{4b}	RIM1	−27.8 ± 4.9 (18)*	−9.1 ± 1.6 (13)	5.6 ± 0.2 (13)	0.59 ± 0.04 (13)	0.70 ± 0.04 (6)***	−21.3 ± 1.2 (6)***	−5.6 ± 0.7 (6)			
$Ca_v2.2$	Vector	−50.8 ± 11.9 (12)	−4.1 ± 1.0 (11)	6.8 ± 0.2 (11)	0.67 ± 0.06 (11)	0.91 ± 0.03 (7)	−64.5 ± 1.6 (7)	−7.8 ± 0.5 (7)	0.09 ± 0.04 (7)	−22.4 ± 2.1 (7)	−5.1 ± 1.7 (7)
+ β_{4b}	RIM1	−96.4 ± 18.5 (10)*	−7.0 ± 1.0 (7)	6.8 ± 0.4 (7)	0.73 ± 0.02 (7)	0.30 ± 0.06 (5)***	−59.7 ± 1.2 (5)	−7.7 ± 0.7 (5)	0.61 ± 0.06 (5)***	−20.8 ± 1.8 (5)	−4.9 ± 1.0 (5)
$Ca_v2.3$	Vector	−23.0 ± 7.7 (10)	−10.3 ± 1.5 (7)	8.4 ± 0.5 (7)	0.47 ± 0.03 (7)	0.91 ± 0.02 (5)	−78.2 ± 1.3 (5)	−6.7 ± 0.7 (5)	0.08 ± 0.04 (5)	−36.2 ± 3.3 (5)	−6.1 ± 2.9 (5)
+ β_{4b}	RIM1	−23.4 ± 5.4 (12)	−5.3 ± 1.4 (6)*	9.4 ± 0.6 (6)	0.67 ± 0.07 (6)*	0.35 ± 0.05 (6)***	−71.0 ± 1.6 (6)*	−9.1 ± 0.9 (6)	0.53 ± 0.05 (6)***	−27.9 ± 2.3 (6)	−7.5 ± 0.4 (6)
$Ca_v1.2$	Vector	−18.6 ± 3.6 (10)	−13.6 ± 1.3(12)	8.4 ± 0.4 (12)	0.46 ± 0.03 (6)	0.93 ± 0.02 (6)	−24.6 ± 3.1 (6)	−8.3 ± 1.3 (6)			
+ β_{4b}	RIM1	−17.1 ± 2.3 (13)	−8.0 ± 1.3 (11)**	10.2± 0.3 (11)**	0.62 ± 0.04 (7)*	0.75 ± 0.07 (5)*	−24.7 ± 1.6 (5)	−10.1 ± 0.6 (5)			

1) $^{*}P < 0.05$, $^{**}P < 0.01$, $^{***}P < 0.001$ vs vector.

2) Ba^{2+} currents evoked by depolarizing pulse to 0 mV from a V_h of −100 or −110 mV are divided by capacitance.

3) Activation time constants obtained from currents elicited by 5-ms test pulse to 20 mV. The activation phases are well fitted by a single exponential function.

Supplementary Table 2 Effects of RIM1 constructs on current density, activation, and inactivation of $Ca_v2.1$ channel in BHK cells expressing α_2/δ and various β-subunits[1].

Subunit combination		Current density (pA / pF)[2]	Activation parameters			Inactivation parameters		
			$V_{0.5}$ (mV)	k (mV)	τ_{act} (ms)[3]	a	$V_{0.5}$ (mV)	k (mV)
$Ca_v2.1$	Vector	−30.0 ± 4.4 (11)	−12.3 ± 1.0 (6)	5.0 ± 0.2 (6)	0.35 ± 0.04 (5)	1.00 ± 0.00 (7)	−62.6 ± 1.9 (7)	−7.0 ± 0.3 (7)
+ β_{1a}	RIM1	−31.1 ± 5.5 (7)	−12.0 ± 0.7 (7)	4.9 ± 0.2 (7)	0.49 ± 0.04 (6)*	0.83 ± 0.07 (5)***	−21.6 ± 2.5 (5)***	−6.1 ± 0.9 (5)
+ β_{2a}	Vector	−30.0 ± 5.8 (15)	−10.3 ± 0.9 (8)	5.0 ± 0.2 (8)	0.45 ± 0.03 (8)	1.00 ± 0.00 (13)	−47.4 ± 0.9 (13)	−6.2 ± 0.2 (13)
	RIM1	−22.7 ± 3.7 (6)	−6.0 ± 0.5 (6)***	5.4 ± 0.2 (6)	0.65 ± 0.02 (6)***	0.73 ± 0.05 (6)***	−18.4 ± 1.4 (6)***	−5.3 ± 0.6 (6)
+ β_3	Vector	−19.9 ± 3.6 (16)	−11.3 ± 0.6 (8)	5.0 ± 0.3 (8)	0.50 ± 0.05 (8)	1.00 ± 0.00 (7)	−67.5 ± 1.4 (7)	−6.8 ± 0.3 (7)
	RIM1	−22.5 ± 3.6 (23)	−9.2 ± 1.3 (9)	5.6 ± 0.2 (9)	0.74 ± 0.07 (7)*	0.66 ± 0.05 (5)***	−13.2 ± 3.3 (5)***	−6.0 ± 0.5 (5)
+ β_{4b}	Vector	−14.0 ± 2.9 (15)	−7.2 ± 1.2 (9)	5.7 ± 0.1 (9)	0.53 ± 0.05 (9)	1.00 ± 0.00 (12)	−45.9 ± 1.8 (12)	−7.5 ± 0.3 (12)
	RIM1	−27.8 ± 4.9 (18)*	−9.1 ± 1.6 (13)	5.6 ± 0.2 (13)	0.59 ± 0.04 (13)	0.70 ± 0.04 (6)***	−21.3 ± 1.2 (6)***	−5.6 ± 0.7 (6)
	RIM1(1079–1463)	−29.9 ± 5.0 (10)*						

1) $^{*}P < 0.05$, $^{***}P < 0.001$ vs vector.

2) Ba^{2+} currents evoked by depolarizing pulse to 0 mV from a V_h of –100 mV are divided by capacitance.

3) Activation time constants obtained from currents elicited by 5-ms test pulse to 20 mV. The activation phases are well fitted by a single exponential function.

Supplementary Table 3 Effects of RIM1 or C-terminal truncated mutants of RIM1 on inactivation of $Ca_v2.1$ channel in BHK cells expressing α_2/δ and β_{1a}[1)2)].

	Inactivation parameters					
	a	$V_{0.5}^{1st}$ (mV)	k^{1st} (mV)	*b*	$V_{0.5}^{2nd}$ (mV)	k^{2nd} (mV)
Vector	1.00 ± 0.00 (7)	−62.6 ± 1.9 (7)	−7.0 ± 0.3 (7)			
RIM1	0.83 ± 0.07 (5)**	−21.6 ± 2.5 (5)***	−6.1 ± 0.9 (5)			
RIM1(1079–1257)	1.00 ± 0.00 (4)#	−58.9 ± 0.7 (4)###	−8.0 ± 0.8 (4)			
RIM1(1258–1463)	0.51 ± 0.03 (6)***###	−55.2 ± 1.5 (6)*###	−9.6 ± 0.9 (6)*##	0.41 ± 0.02 (6)	−22.3 ± 1.0 (6)	−5.1 ± 0.9 (6)
RIM1(1079–1463)	0.70 ± 0.05 (5)***#	−15.8 ± 3.7 (5)***	−5.9 ± 0.9 (5)			

1) $^{*}P < 0.05$, $^{**}P < 0.01$, $^{***}P < 0.001$ vs vector.

2) $^{\#}P < 0.05$, $^{\#\#}P < 0.01$, $^{\#\#\#}P < 0.001$ vs RIM1.

Supplementary Table 4 Effects of RIM1 on inactivation of $Ca_v2.2$ channel in BHK cells expressing α_2/δ and β_4-GK.

	Inactivation parameters					
	a	$V_{0.5}^{1st}$ (mV)	k^{1st} (mV)	*b*	$V_{0.5}^{2nd}$ (mV)	k^{2nd} (mV)
Vector	0.75 ± 0.08 (5)	−48.9 ± 1.5 (5)	−8.1 ± 0.6 (5)	0.20 ± 0.05 (5)	−5.0 ± 2.2 (5)	−3.9 ± 1.0 (5)
RIM1	0.78 ± 0.07 (5)	−44.0 ± 1.8 (5)	−8.1 ± 0.6 (5)	0.11 ± 0.05 (5)	1.4 ± 0.4 (5)	−4.5 ± 0.4 (5)

Supplementary Table 5 Effects of RIM1 or BADN on inactivation of $Ca_v2.1$ channel in BHK cells expressing α_2/δ and β_{1a}.

	Inactivation parameters					
	a	$V_{0.5}^{1st}$ (mV)	k^{1st} (mV)	*b*	$V_{0.5}^{2nd}$ (mV)	k^{2nd} (mV)
RIM1	0.06 ± 0.02 (4)***	−64.3 ± 1.9 (4)	−3.8 ± 0.8 (4)**	0.73 ± 0.07 (4)	−22.3 ± 0.9 (4)	−5.1 ± 0.8 (4)
Vector	1.00 ± 0.00 (6)	−62.0 ± 3.1 (6)	−6.7 ± 0.2 (6)			
RIM1 + BADN	0.73 ± 0.08 (5)***###	−64.6 ± 2.4 (5)	−6.0 ± 0.8 (5)#	0.24 ± 0.06 (5)**	−29.2 ± 3.8 (5)	−8.4 ± 2.8 (5)

1) $^{**}P < 0.01$, $^{***}P < 0.001$ vs vector.

2) $^{\#}P < 0.05$, $^{\#\#\#}P < 0.001$ vs RIM1.

Supplementary Table 6 Effects of RIM1 on inactivation of $Ca_v2.1$ channel in HEK cells expressing α_2/δ and β_1[1)].

	Inactivation parameters					
	a	$V_{0.5}^{1st}$ (mV)	k^{1st} (mV)	*b*	$V_{0.5}^{2nd}$ (mV)	k^{2nd} (mV)
Vector (Ca^{2+})	1.00 ± 0.00 (5)	−41.0 ± 0.7 (5)	−5.8 ± 0.3 (5)			
RIM1 (Ca^{2+})	0.22 ± 0.05 (5)***	−35.5 ± 1.7 (5)	−7.4 ± 1.1 (5)	0.79 ± 0.05 (5)	−10.8 ± 1.4 (5)	−3.0 ± 0.2 (5)
Vector (Ba^{2+})	1.00 ± 0.00 (5)	−48.5 ± 1.0 (5)	−5.8 ± 0.3 (5)			
RIM1 (Ba^{2+})	0.23 ± 0.02 (5)***	−45.5 ± 2.4 (5)	−6.4 ± 0.6 (5)	0.58 ± 0.01 (5)	−16.3 ± 1.7 (5)	−4.0 ± 0.6 (5)

1) $^{***}P < 0.001$ vs vector

Supplementary Table 7 Effects of RIM1 or BADN on inactivation of VDCCs in PC12 cells[1)2)].

	Inactivation parameters					
	a	$V_{0.5}^{1st}$ (mV)	k^{1st} (mV)	*b*	$V_{0.5}^{2nd}$ (mV)	k^{2nd} (mV)
Vector	0.23 ± 0.04 (5)	−42.7 ± 0.6 (5)	−7.0 ± 0.9 (5)	0.48 ± 0.04 (5)	−6.9 ± 0.9 (5)	−5.2 ± 0.5 (5)
RIM1	0.07 ± 0.01 (5)**	−40.7 ± 4.5 (5)	−6.4 ± 2.3 (5)	0.54 ± 0.03 (5)	−7.7 ± 1.3 (5)	−5.3 ± 0.4 (5)
BADN	0.36 ± 0.03 (6)**###	−48.5 ± 2.6 (6)	−7.8 ± 0.7 (6)	0.48 ± 0.04 (6)	−11.7 ± 1.3 (6)*#	−5.5 ± 0.6 (6)
siControl	0.21 ± 0.04 (6)	−36.8 ± 1.7 (6)	−7.9 ± 1.4 (6)	0.37 ± 0.04 (6)	−5.3 ± 1.0 (6)	−3.9 ± 0.5 (6)
siRIM1 and RIM2	0.39 ± 0.04 (8)**	−38.6 ± 1.8 (8)	−8.4 ± 0.6 (8)	0.32 ± 0.02 (8)	−6.4 ± 1.5 (8)	−5.1 ± 0.6 (8)

1) $^{*}P < 0.05$, $^{**}P < 0.01$ vs vector.

2) $^{\#}P < 0.05$, $^{\#\#\#}P < 0.001$ vs RIM1.

Supplementary Table 8 Buffer solutions for biochemistry.

Buffer Name	Constituents (final concentration):
NP40 buffer	150 mM NaCl, 50 mM Tris, 1 % NP40, protease inhibitors (1 mM PMSF, 10 μg/ml leupeptin), pH 8.0
Buffer I	50 mM Tris, 500 mM NaCl, 1 % digitonin, protease inhibitors (0.6 μg/mL pepstatin A, 0.5 μg/mL aprotonin and leupeptin, 0.1 mM PMSF, 0.75 mM benzamidine, 2 μM calpain I inhibitor and calpeptin), pH 7.4
Buffer II	20 mM HEPES, 300 mM NaCl, 0.1 % digitonin, protease inhibitors (same as buffer I), pH 7.4
Buffer III	20 mM HEPES, 400 mM NaCl, 0.1 % digitonin, protease inhibitors (same as buffer I), pH 7.4
Buffer IV	20 mM HEPES, 700 mM NaCl, 0.1 % digitonin, protease inhibitors (same as buffer I), pH 7.4
Buffer V	20 mM HEPES, 0.1 % digitonin, protease inhibitors (same as buffer I), pH 7.4
Buffer VI	50 mM Tris, 150 mM NaCl, 0.1 % digitonin, protease inhibitors (same as buffer I), 5 – 40% sucrose, pH 7.4

Supplementary Table 9 Antisense and sense PCR primers.

Gene	Orientation	Pair of primers for first PCR (5' to 3')	Pair of primers for nested PCR (5' to 3')
$Ca_v1.2$	Sense	AAGAAGAGAAGGAGAGAAAGAAGCTGGC	GATGCGGAGAGCCTGACCTCTGCCC
	Antisense	CATCCTCTTCACCTGCAGTGTCTGGG	CGGGGGCGTGGGCCCACAGGCATCTCG
$Ca_v1.3$	Sense	TGAGACACAGACCAAGCGAAGC	ACCTTCGACAACTTCCCACAGGCGCTCC
	Antisense	GTTGTCACTGTTGGCTATCTGG	GACCTCTGGTTTGTTGTTTTTTTTGTTTTCTAGG
$Ca_v1.4$	Sense	TCTTCATGCTCTGTGCCT	CCTAACCAGAGATTGGTCTATTCTGGGACCC
	Antisense	AGCCCTGCCTGGTCCTGA	CCTGGGATGGGCAAATCCTCACAACTGCCC
$Ca_v2.1$	Sense	CCAGTCTGTGGAGATGAGAGAAATGGG	CTGATGGCTACTCAGACAGCGAACACTACC
	Antisense	TTTGGAGGGCAGGTCACCCGATTG	CATGCTCAGATCTGTCCCCAGGCC
$Ca_v2.2$	Sense	GCCGTCTCAGCCGCGGCCTTTCT	CAATGCCCTGCTCCAGAAAGAGCCC
	Antisense	CAAAGGTGAGTGTATCCTCAGGC	CCAGACGCTGCCCTAGGTAAGGGTC
$Ca_v2.3$	Sense	ATCTTACTGTGGACCTTCGTGC	GCAGTCCTTTAAGGCTCTCCCCTATG
	Antisense	CTAGCGGTGGTGACATGAGAGTCAGC	CATACATCTCAGTGTAATGGATGCGGCC
β_1	Sense	TCCAGGGACCCTACCTTGTTTCC	GGGACCAGCCGCTGGACCGGG
	Antisense	CCTCCAGCTCATTCTTATTGCGC	GGCCCACCACCCTCCGCACAG
β_2	Sense	TCGGATCCGAAGAAGAACCTTGTCTGG	CCCAACACCGTTCTTCCTCAGCCACACACC
	Antisense	TCGAATTCAGTAGCGATCCTTAGATTTATGC	CCTAGTGCGGTGGCGAGGCTCC
β_3	Sense	GTGGTGTTGGATGCTGAC	GCACAGCTAGCCAAGACCTCACTGG
	Antisense	ATTGTGGTCATGCTCCGA	GGTCATGCCCGTTAGCACTGGG
β_4	Sense	CGTGGGCTCCACAGCTCTCTCACC	CTCTGGACTACAGAGTCAGCGGATGAGGC
	Antisense	CCACCAGAGGGTAGTGATCTCGGCTGTGC	GGAGGACAAGCGGTTCCTACTCTTGCGG
RIM1	Sense	CAGCATCAACAGTTATAGCTCGG	
	Antisense	CATCCAATCACCATGCTGGATAG	
RIM2	Sense	GGATCACAAATCCTTTATGGGAGTGG	
	Antisense	CACAGGATGGCTCTTTATCCCTAGAC	
β-actin	Sense	TTCTACAATGAGCTGCGTGTGGC	
	Antisense	CTCATAGCTCTTCTCCAGGGAGGA	
β-lactamase	Sense	GTTACATCGAACTGGATCTCAACAGC	
	Antisense	CGTGTAGATAACTACGATACGGGAG	

Supplementary Methods

cDNA cloning and construction of expression vectors

RIM1 (NM_053270) was cloned from mouse brain Marathon-Ready cDNA (Clontech) using PCR, and was subcloned into pCI-neo (Promega), the FLAG-tagged vector pCMV-tag2 (Stratagene), the myc-tagged vector pCMV-tag3 (Stratagene), the pDsRed-Monomer-N1 (Clontech), and the pIRES2-EGFP (Clontech). Rat β_{4b} (XM_215742) was subcloned into the same vectors. The rat β_{4b} construct, BADN, that carries ELNG (amino acid residues 388-391 of rabbit Cav2.1) with G flanking on both the N- and C-terminal sides for ENQ (380-382 of rat β_{4b}) (**Supplementary Fig.3**), was created by using PCR, and was subcloned into PCI-neo. $Ca_v2.1$(I-II linker) (1-435) was constructed by PCR using pK4KBI-2 (ref. 1), and was subcloned into pCMV-tag2. Mouse VAMP (NM_009497) was cloned using PCR from mouse brain Marathon-Ready cDNA (Clontech), and was subcloned into pEGFP-N1 (Clontech). Human caveolin-1 (NM_001753) was cloned using PCR from human lung Marathon-Ready cDNA (Clontech), and was subcloned into pEGFP-N1 (Clontech). Expression plasmids pGBK-T7 carrying β_{4b} or its mutants were constructed by PCR.

Cell culture and cDNA expression in HEK293 cells

HEK293 cells were cultured in Dulbecco's modified Eagle's medium (DMEM) containing 10% fetal bovine serum, 30 units/ml penicillin, and 30 μg/ml streptomycin. Transfection of cDNA plasmids was carried out using SuperFect Transfection Reagent (QIAGEN). The cells were subjected to electrophysiological measurements and confocal imaging 48-72 h after transfection.

cDNA expression of Ca^{2+} channels in BHK cells

Rabbit β_{2a}-subunit (X64297) and rabbit β_3-subunit (X64300) were subcloned into pCI-neo to yield pCI-β_{2a} and pCI-β_3, respectively. BHK cells cultured as previously described[2] were transfected with pAGS-3a2 and pCI-β_{2a} or pCI-β_3 using SuperFect (Qiagen), and were cultured in DMEM containing Geneticin (600 μg/ml) (Sigma) and Zeocin (600 μg/ml) (invitrogen), to establish BHK lines stably expressing α_2/δ and β_{2a}, or β_3. BHK lines stably expressing α_2/δ and β_{1a}, or β_{4b} and BHK6-2 stably expressing $Ca_v2.1$, α_2/δ and β_{1a} were described previously[2]. These BHK cell lines were co-transfected with pK4K plasmids containing cDNAs for α_1-subunits (pK4KBI-2, pK4KBII, pK4KBIII, pK4KC1) and expression plasmids carrying RIM1 constructs (pIRES2-EGFP-vector, pIRES2-EGFP-RIM1, pIRES2-EGFP-RIM1(1079-1463), pIRES2-EGFP-RIM1(1079-1257), pIRES2-EGFP-RIM1(1258-1463)), using Effectene Transfection Regent (Qiagen). The cells were subjected to measurements 72-96 h after transfection.

Production of GST fusion proteins and purified recombinat β_4-subunit proteins.

For production of GST fusion proteins for RIM1, cDNAs for RIM1 constructs and the GST were subcloned together into the pET23 vector (Novagen). The Rosetta strain (Novagen) of *Escherichia coli* was transformed by the expression vectors, and protein expression/purification was performed according to the manufacturer's instruction (Novagen, GE Healthcare). For production of recombinant β_4-subunits, the gene encoding residues 47-475 of rat β_{4b}-subunit and the GST were subcloned into the pET23 vector (Novagen). The GST-β_4 proteins were purified by

glutathione-Sepharose affinity column (GE Healthcare), and the GST tag was cleaved by incubation with thrombin (4 units/ml, Sigma) for 6 h at 4 °C. Resultant GST and thrombin were removed by glutathione-Sepharose and benzamidine-beads (Sigma) to obtain purified recombinant β_4-subunits. The purified recombinant of residues 47-410 (for disruption experiments) or 47-475 (for *in vitro* binding assay) of BADN was obtained using the same protocol as that for the β_4-subunit. These proteins were stored at –80 °C.

Molecular modeling of BADN

Molecular building and molecular dynamics calculations were performed with Insight II / Discover packaged in the context of the Molecular Simulations Inc (MSI) under the consistent valence force field (CVFF). Biopolymer modules based on the X-ray crystallographic data of β_2-subunit and AID complex (PDB ID: 1T3L) in RSCB protein data bank (PDB) were used. During molecular dynamics minimization around 1000 K, most of the structure except for hexa-peptide (GELNGG, see **Supplementary Fig. 3b**) was restrained. An energetically stabilized conformation was chosen.

***in vitro* binding of the purified RIM1 GST fusion and recombinant β_4 proteins**

RIM1 GST fusion proteins at various concentrations were incubated with 50 pM purified recombinant β_4-subunits for 3 h at 4 °C in PBS buffer containing 0.1 % NP40 and 50 μg/ml BSA, and then with glutathione-Sepharose beads for 1 h. The beads were centrifuged and washed twice with the PBS buffer. Proteins were boiled in SDS sample buffer and subject to 10 % SDS-PAGE, followed by western blotting (WB) with the anti-β_4 antibody raised against the peptide containing ENYHNERARKSRNRLS,

and detected by enhanced chemiluminescence (Pierce). The densities of protein signals, obtained using NIH image under the linear relationship with the applied amount of proteins (**Supplementary Fig. 2a**), were normalized to the densities from the maximal binding. Three independent experiments were performed.

GST-pulldown assay, and coimmunoprecipitation in HEK293 cells.

48 h after transfection, HEK293 cells were solubilized in NP40 buffer (**Supplementary Table 8**), then centrifuged at 17400 x *g* for 20 min. For pulldown assay, the cell lysate was incubated with glutathione-Sepharose beads bound with purified fusion proteins, then the beads were washed with NP40 buffer at 4 °C. The proteins retained on the beads were characterized by WB with anti-myc antibody (invitrogen). For coimmunoprecipitation, the cell lysate was incubated with anti-FLAG M2 monoclonal antibody (Sigma), then the immunocomplexes were incubated with protein A-agarose beads (Santa Cruz) and washed with NP40 buffer. Immunoprecipitated proteins were characterized by WB with anti-myc antibody.

Confocal imaging

PC12 cells were cultured as described previously[3]. 32 h after transfection, HEK293 cells or PC12 cells were plated onto poly-L-lysine coated glass coverslips. 56 h after transfection, Hoechst 33342 (1 μg/ml, Dojindo) was added for 30 min to stain nuclei. The imaging was performed in modified Ringer's buffer that contained (in mM): 130 NaCl, 3 KCl, 5 $CaCl_2$, 1.5 $MgCl_2$, 10 glucose, 10 HEPES (pH 7.4). Fluorescence images were acquired with a confocal laser-scanning microscope (Olympus FV500) using the 405-nm line of an laser diode for excitation and a 430-nm to 460-nm

band-pass filter for emission (Hoechst 33342), the 488-nm line of an argon laser for excitation and a 505-nm to 525-nm band-pass filter for emission (EGFP or Venus), or the 543-nm line of a HeNe laser for excitation and a 560-nm long-pass filter for emission (DsRedmonomer). The specimens were viewed at high magnification using plan oil objectives (x60, 1.40 numerical aperture (NA), Olympus).

Total internal reflection fluorescence (TIRF) microscopy

PC12 cells co-transfected with 1 μg pVenus-N1-NPY and of expression plasmids for RIM1 constructs at the equal molar quantity (5.0 μg of RIM1(11-399), 5.7 μg of RIM1(400-1078), 5.0 μg of RIM1(1079-1463), or 7.5 μg of RIM1) and BADN (10 μg) using OptiFect (invitrogen) were plated onto poly-L-lysine-coated coverslips. PCR analysis of the transfection level reveals that the RIM plasmids are transfected at the equal level (**Supplemetary Fig. 7b**). The imaging was performed in modified Ringer's buffer. Fluorescence images of NPY-Venus were observed at the single vesicle level as previously reported[4]. In brief, a high numerical aperture objective lens (Plan Apochromatic, 100x, numerical aperture = 1.45, infinity-corrected, Olympus) was mounted on an inverted microscope (IX71, Olympus), and incident light for total internal reflection illumination was introduced from the high numerical objective lens through a single mode optical fiber. A diode-pumped solid state 488-nm laser (kyma488, 20 milliwatt, MELLES GRIOT) was used for total internal fluorescence illumination and 510-nm long pass filter as an emission filter. Images were captured by a cooled CCD camera (EM-CCD, Hamamatsu Photonics) operated with Metamorph (Molecular Devices). Area calculations and counting the number of fluorescent spots were performed using Metamorph softwares. We omitted the cells with disruption of

distribution of vesicles by a dark spot with area > 10 μm^2 were omitted, to select the cells, in which vesicles were uniformly distributed, for the analyses. 10 μm^2 was adopted, because 10 μm^2 was the maximal dark circle area that can be located in between vesicles in the images from BADN-transfected cells with uniform vesicle distribution. The statistical analyses were performed using ANOVA followed by Fisher's test.

Quantification of presynaptic $Ca_v2.1$ accumulation

For quantification of $Ca_v2.1$ accumulation at presynaptic varicosities, neurons were co-transfected, at 6 or 7 DIV, with EGFP-tagged $Ca_v2.1$ and mCherry. Immunofluorescent z-stack images for EGFP and mCherry were acquired using a Zeiss LSM510META confocal microscope, and a projection image was obtained from each of confocal z-stack images for EGFP and mCherry using a simple summation algorithm in order to retain all pixel fluorescence information. Somata and varicosities were manually cropped on the projection image of mCherry fluorescence to define individual regions of interests (ROIs). At least 10 adjacent varicosities were selected from a randomly chosen axonal process that could be traced directly from a mCherry-positive soma. Subsequently, fluorescence values of all pixels within each ROI in the image were integrated to calculate the total fluorescence for EGFP-$Ca_v2.1$ and mCherry. Integrated fluorescence at each varicosity was then normalized by dividing against the integrated soma fluorescence, in order to estimate the relative expression per each varicosity. Because this "relative expression factor" is heavily dependent on the sizes of the varicosities and the soma, we further calculated a ratio between the "relative expression factor" for $Ca_v2.1$ and the "relative expression factor" for mCherry at each

varicosity, and designated the ratio as "$Ca_v2.1$ accumulation index". Since mCherry is a space-filling volume marker, this ratio is indicative of volume-independent $Ca_v2.1$ enrichment at each varicosity. Statistical analysis was carried out by a Kolmogorov-Smirnov test between either 22 DIV and + RIM1(1079-1463) samples, or between 22 DIV and + BADN samples.

Current recordings

Whole-cell mode of the patch-clamp technique was performed on BHK cells or PC12 cells at room temperature (22-25 °C) as previously described[2]. Pipette resistance ranged from 2 to 3.5 megohm. The series resistance was electronically compensated, and both the leakage and the remaining capacitance were subtracted by a –P/4 method. Currents were sampled at 100 kHz after low pass filtering at 8.4 kHz (3 db) in the experiments of activation kinetics, otherwise sampled at 10 kHz after low pass filtering at 2.9 kHz (3 db). An external solution contained (in mM): 3 $BaCl_2$, 155 tetraethylammonium chloride (TEA-Cl), 10 HEPES, 10 glucose (pH adjusted to 7.4 with tetraethylammonium-OH). For current recordings in PC12 cells, an external solution contained (in mM): 10 $BaCl_2$, 153 TEA-Cl, 10 HEPES, 10 glucose (pH adjusted to 7.4 with TEA-OH). The pipette solution contained (in mM): 95 CsOH, 95 Aspartate, 40 CsCl, 4 $MgCl_2$, 5 EGTA, 2 $ATPNa_2$, 5 HEPES, 8 creatine phosphate (pH adjusted to 7.2 with CsOH). To characterize Ca^{2+}-dependent inactivation of $Ca_v2.1$ expressed in HEK293 cells, external solutions contained (in mM): 5 $CaCl_2$ or $BaCl_2$, 153 TEA-Cl, 10 HEPES, 10 glucose (pH adjusted to 7.4 with tetraethylammonium-OH (TEA-OH)). The pipette solution contained (in mM): 135 Cs-$MeSO_3$, 5 CsCl, 0.5 EGTA, 5 $MgCl_2$, 4 $ATPNa_2$ and 10 HEPES (pH adjusted to 7.2 with CsOH).

Single-channel currents were recored using cell-attached patch mode[2]. Patch electrodes had resistance of 5-8 megohms. The bath solution contained (in mM): 150 KCl, 5 HEPES, 0.2 EGTA, 10 glucose (pH adjusted to 7.4 with KOH). The pipette solution contained (in mM): 110 $BaCl_2$ and 10 HEPES (pH adjusted to 7.4 with $Ba(OH)_2$). Voltage steps with duration of 750 ms were given every 5 s from a V_h of –100 mV. The data, low-passed filtered at 1 kHz (3 db, 8-pole Bessel filter), were digitized at 10 kHz and analyzed using the pCLAMP 6.02 software. The records were corrected for capacitative and leakage currents by subtraction of the average of records without channel activity.

Voltage dependence of inactivation

To determine the voltage dependence of inactivation (inactivation curve) of VDCCs, Ba^{2+} currents were evoked by 20-ms test pulse to 5 mV after the 10-ms repolarization to –100 mV (–110 mV for $Ca_v2.3$, –80 mV for PC12) following 2-s V_h displacement (conditioning pulse) from –110 mV to 20 mV (from –80 mV to 20 mV for PC12) with 10-mV increments. Amplitudes of currents elicited by the test pulses were normalized to those elicited by the test pulse after a 2-s V_h displacement to –110 mV (–80mV for PC12). The mean values were plotted against potentials of the 2-s V_h displacement. When the inactivation curve was monophasic, the mean values were fitted to the single Boltzmann's equation:

$$h(V_h) = (1-a)+a\ /\{1+\exp[(V_{0.5}{}^{1st}-V_h)/k^{1st}]\}$$

where a is the rate of inactivating component, $V_{0.5}{}^{1st}$ is the potential to give a half-value of inactivation, and k^{1st} is the slope factor. Otherwise, the mean values were fitted to the sum of two (1^{st} and 2^{nd}) Boltzmann's equations:

$h(V_h) = (1–a–b)+a/\{1+\exp[(V_{0.5}{}^{1st}–V_h)/k^{1st}]\}+b\{1+\exp[(V_{0.5}{}^{2nd}–V_h)/k^{2nd}]\}$

where a and b are the ratios of 1st and 2nd inactivating phases, $V_{0.5}{}^{1st}$ and $V_{0.5}{}^{2nd}$ are the potentials give a half-value of 1st and 2nd inactivation phases, and k^{1st} and k^{2nd} are the slope factors for 1st and 2nd inactivating phases, respectively.

The AP train was the same as Patil *et al.*[5]. APs began at −80 mV and peaked at 33 mV. Maximal rising and falling slopes were 300 V/s and −100 V/s, respectively. Leaks and capacitive transients were subtracted by a –P/6 protocol. External solution contained 3 mM Ba^{2+}.

Voltage dependence of activation

Tail currents were elicited by repolarization to –60 mV after 5-ms test pulse from –50 to 50 mV with 5-mV increments. Currents were sampled at 100 kHz after low pass filtering at 8.4 kHz. Amplitude of tail currents were normalized to the tail current amplitude obtained with a test pulse to 50 mV. The mean values were plotted against test pulse potentials, and fitted to the Boltzmann's equation:

$n(V_m) = 1/\{1+\exp[(V_{0.5}–V_m)/k]\}$

where V_m is membrane potential, $V_{0.5}$ is the potential to give a half-value of conductance, and k is the slope factor.

Release assay and RNA analysis in PC12 cells

RNA expression of the α_1-subunits, β-subunits, RIM1, or RIM2 in PC12 cells was determined by RT-PCR (**Supplemetary Fig. 7a,c**) using specific primers listed in **Supplementary Table 9**. ACh secretion experiments were performed as previously reported with slight modifications[3]. PC12 cells were plated in poly-D-lysine-coated

35-mm dishes (BD bioscience) with 5 x 10^5 cells per dish. Cells were co-transfected with 1 μg of pEFmChAT encoding mouse ChAT cDNA and RIM1 plasmids at equal molar quantity (3.4 μg of RIM1(11-399), 3.8 μg of RIM1(400-1078), 3.4 μg of RIM1(1079-1463), or 5.0 μg of RIM1) and BADN (10 μg) using Lipofectamine^{TM} 2000 (invitrogen). Three days after transfection, PC12 cells were washed with a low-K^+ solution that contained (in mM): 0.01 eserine, 140 NaCl, 4.7 KCl, 1.2 KH_2PO_4, 2.5 $CaCl_2$, 1.2 $MgSO_4$, 11 glucose, 15 HEPES-NaOH (pH 7.4) and incubated for 30 s with the low-K^+ solution at 37 °C. The release of ACh during this period was considered as basal release. To measure K^+-stimulated release of ACh, the cells were then incubated for 30 s with a high-K^+ solution that contained (in mM): 0.01 eserine, 94.8 NaCl, 49.9 KCl, 1.2 KH_2PO_4, 2.5 $CaCl_2$, 1.2 $MgSO_4$, 11 glucose, 15 HEPES-NaOH (pH 7.4). Supernatant from cells solubilized in NP40 buffer and centrifuged at 17400 x *g* for 20 min at 4 °C was taken as the cellular ACh that was not secreted. ACh was measured using HPLC with electrochemical detection (HTEC-500, EiCOM). ANOVA followed by Fisher's test was employed for statistical analyses.

Suppression of the action of endogenous RIM1 and RIM2 using specific siRNAs and BADN in PC12 cells

The sense siRNA sequences 5'-AAGAATGGACCACAAATGCTT-3' and 5'-AAGGTGATTGGATGGTATAAA-3' for rat RIM1, and 5'-AAGGCCCAGATACTCTTAGAT-3' and 5'-AAGAACTATCCAACATGGTAA-3' for rat RIM2 were used. To construct siRNA oligomers, the Silencer siRNA Construction Kit (Ambion) was used. The GAPDH siRNA (siControl) used was the control provided with the kit. We transfected the mixture of RIM1 and RIM2 siRNAs

to PC12 cells using Lipofectamine^{TM} 2000. Suppression of RNA expression was confirmed using RT-PCR analyses (**Supplemetary Fig. 7a**). 8.0 μg pCI-neo-BADN or 8.0 μg pCI-neo-RIM1 was transfected as described above in the TIRF imaging. The cells treated with siRNAs or cDNA constructs were subjected to patch clamp measurements 72-96 h after transfection.

Preparation of cerebellar neuron primary cultures

As described previously[6], following decapitation of 7–9-day-old Wister rats, cerebella were removed and transferred into ice-cold DMEM immediately. After eliminating meninges, the tissues were cut into 1-mm pieces and incubated in PBS containing 1% (w/v) trypsine (Difco), 12.5 mM glucose (Difco), 0.02 % (w/v) DNase (Sigma) for 20 min at 37 °C, with occasional agitation. The trypsin solution was removed after a brief centrifugation and the tissue was mechanically dissociated by repeated pipetting in DMEM containing 10 % (v/v) FCS (GIBCO). The cell suspension obtained was left for 10 min at room temperature to let the remaining tissues precipitate. The cell suspension was then collected carefully and spun at 200 x *g* for 3 min. After washing once by centrifugation, the pellet was resuspended in 10 ml of culture medium composed of DMEM with 10 % FCS, 26 mM KCl, 60 U/ml penicillin, and 60 μg/ml streptomycin. After filtering through a cell strainer (70 μm, BD Falcon), the cells were plated on polyethylenimine-coated 35-mm diameter culture dishes (BD Falcon) at a density of 4.5–5.0 x 10^6 cells/dish, and maintained at 37 °C in 10 % CO_2. Between 2 and 4 DIV, the medium was replaced with fresh medium containing 1 μM cytosine arabinofuranoside to inhibit the replication of non-neuronal cells, and thereafter no further medium change was carried out before experiments.

Preparation and infection of Sindbis viruses

The plasmid pSinEGdsp/BADN and pSinEGdsp/RIM1 were generated from the plasmid pSinEGdsp (kindly provided by S. Ozawa) containing the second subgenomic promoter followed by the cDNA of GFP[7]. The cDNA of BADN or RIM1 was ligated into the cloning site immediately downstream of the first subgenomic promoter. The recombinant RNA was transcribed from the linearized pSinEGdsp, pSinEGdsp/BADN or pSinEGdsp/RIM1 with an InvitroScript CAP SP6 *in vitro* transcription kit (Ambion). This recombinant RNA was co-transfected together with 'helper' RNA encoding the structural proteins of the Sindbis virus into BHK cells using the Gene Pulser II electroporation system (Bio-Rad Laboratories). The virions thus produced and released into the extracellular medium were harvested 36-48 h postinfection and centrifuged at 128690 x *g* for 3 h. The pellet was resuspended with PBS and kept at –80 °C. Cerebellar neurons were infected with recombinant Sindbis viruses on 8–10 div. By 48 h after the infection, 60–80% of the neurons appeared positive for EGFP.

Glutamate release assay

As described previously[6], 24 h after the infection with Sindbis viruses, cerebellar neurons (9–11 div) were washed briefly with pre-warmed low-K^+ solution that contained (in mM): 140 NaCl, 4.7 KCl, 1.2 KH_2PO_4, 2.5 $CaCl_2$, 1.2 $MgSO_4$, 11 glucose, and 15 HEPES-NaOH (pH 7.4), and were incubated for 1 min with the low-K^+ solution at 37 °C. The release of Glutamate during this period was considered as basal release. To measure K^+-stimulated release of Glutamate, the cells were then incubated for 1 min with a high-K^+ solution that contained (in mM): 94.8 NaCl, 49.9 KCl, 1.2 KH_2PO_4, 2.5

$CaCl_2$, 1.2 $MgSO_4$, 11 glucose, 15 HEPES-NaOH (pH 7.4). Glutamate was determined by reverse-phase HPLC on an Eicompak SC-5ODS (EiCOM), using precolum derivatization with *o*-phthalaldehyde and electrochemical detection (HTEC-500, EiCOM).

References

1. Niidome T. et al. Stable expression of the neuronal BI (class A) calcium channel in baby hamster kidney cells. *Biochem. Biophys. Res. Commun.* **203**, 1821-1827 (1994).
2. Wakamori, M. et al. Single tottering mutations responsible for the neuropathic phenotype of the P-type calcium channel. *J. Biol. Chem.* **273**, 34857–34867 (1998).
3. Nishiki, T. et al. Comparison of exocytotic mechanisms between acetylcholine- and catecholamine-containing vesicles in rat pheochromocytoma cells. *Biochem. Biophys. Res. Commun.* **239**, 57-62 (1997).
4. Tsuboi, T. & Fukuda, M. Rab3A and Rab27A cooperatively regulate the docking step of dense-core vesicle exocytosis in PC12 cells. *J. Cell Sci.* **119**, 2196-2203 (2006).
5. Patil, P. G., Brody, D. L. & Yue, D. T. Preferential closed-state inactivation of neuronal calcium channels. *Neuron* **20**, 1027-1038 (1998).
6. Koga, T., Kozaki, S. & Takahashi, M. Exocytotic release of alanine from cultured cerebellar neurons. *Brain Res.* **952**, 282-289 (2002).
7. Okada, T. et al. Sindbis viral-mediated expression of Ca^{2+}-permeable AMPA receptors at hippocampal CA1 synapses and induction of NMDA

receptor-independent long-term potentiation. *Eur. J. Neurosci.* **13**, 1635-1643 (2001).